Cytometry
PART A
Journal of the International Society for Advancement of Cytometry

Noninvasive Sorting of Stem Cell Aggregates Based on Intrinsic Markers

D.G. Buschke,[1,2] J.M. Squirrell,[1,2,3] A. Vivekanandan,[2] C.T. Rueden,[2] K.W. Eliceiri,[1,2,3,4] B.M. Ogle[1,2,3,5]*

[1]The Department of Biomedical Engineering, University of Wisconsin-Madison, Wisconsin 53706

[2]The Laboratory for Optical and Computational Instrumentation, University of Wisconsin-Madison, Wisconsin 53706

[3]The Laboratory for Cellular and Molecular Biology, University of Wisconsin-Madison, Wisconsin 53706

[4]Morgridge Institute for Research, University of Wisconsin-Madison, Wisconsin 53706

[5]The Material Science Program, University of Wisconsin-Madison, Wisconsin 53706

Received 8 November 2013; Revised 13 December 2013; Accepted 24 December 2013

Grant sponsor: NSF CAREER, Grant number: 0844537

Grant sponsor: NIH RC1, Grant number: HL100014

Grant sponsor: Coulter Translational Research Award.

Additional Supporting Information may be found in the online version of this article.

*Correspondence to: Brenda M. Ogle, Associate Professor, University of Minnesota-Twin Cities, 7-130 Hasselmo Hall, 312 Church Street SE, Minneapolis, MN 55455. E-mail: ogle@umn.edu

Published online 17 January 2014 in Wiley Online Library (wileyonlinelibrary.com)

DOI: 10.1002/cyto.a.22436

© 2014 International Society for Advancement of Cytometry

ISAC
International Society for Advancement of Cytometry

Abstract

Noninvasive biomarkers hold important potential for the characterization and purification of stem cells because the addition of exogenous labels, probes, or reporters, as well as the disruption of cell-cell and cell-extracellular matrix interactions, can unintentionally but dramatically alter stem cell state. We recently showed that intensity of the intrinsically fluorescent metabolite, nicotinamide adenine dinucleotide (NADH), fluctuates predictably with changes in stem cell viability and differentiation state. Here, we use multiphoton flow cytometry developed in our laboratory to rapidly and noninvasively characterize and purify populations of intact stem cell aggregates based on NADH intensity and assessed the differentiation capacity of sorted populations. We found removal of aggregates with NADH intensity indicative of cell death resulted in a remaining population of aggregates significantly more likely to produce beating cardiomyocytes (26% vs. 8%, $P < 0.05$). Similarly, we found isolation of stem cell aggregates with NADH intensity indicative of future cardiac differentiation gave rise to more aggregates with beating cardiomyocytes at later time points (50% vs. 28%, $P < 0.05$). Further, coupling NADH intensity with gating based on size, enhances the enrichment for EBs capable of giving rise to cardiomyocytes (59% vs. 27%, $P < 0.05$). Thus, we demonstrate that endogenous properties of cell aggregates, such as NADH and size, can serve as gating parameters for large particle sorting devices to purify populations of stem cells or their progeny in a noninvasive manner, leading the way for improved therapeutic applications. © 2014 International Society for Advancement of Cytometry

Key terms

embryroid body; cell aggregate; stem cells; cardiomyocytes; flow cytometry

THE two primary biological properties of stem cells are self-renewal and the capacity to differentiate into multiple cell types. These unique properties distinguish stem cells from lineage-restricted somatic cells and position stem cells to serve as predictive models of development (1,2), pathogenesis (3,4), and drug toxicity (1,2) and, ultimately, to enhance regenerative therapies. For example, embryonic stem cells (ESCs), which originate from the inner cell mass, are used to test the effects of toxins, such as second-hand smoke, on preimplantation development (1). Alternatively, ESCs can be genetically altered to replicate human genetic defects. In particular, an in vitro model of Down Syndrome has been accomplished by incorporating a single human chromosome 21 into murine ES cells (4). Model systems such as these are valuable tools for basic research and useful alternatives to animal models. However, if stem cells (including ESCs, induced pluripotent stem cells, adult hematopoietic stem cells, or adult mesenchymal stem cells) are to be effective in this capacity, or in the context of regenerative therapies, it is imperative that the maintenance and loss of differentiation capacity be tightly regulated and closely monitored.

Most current means to screen or monitor stem cell state rely on the application of extrinsic labels or probes, such as fluorescent molecules bound to antibodies or

peptides, or genetic modification to incorporate reporter molecules. Further, many techniques also require disassociation of stem cells from neighboring cells, as well as from the culture dish or scaffold on which they were initially seeded. These manipulations cause changes in stem cell state (5–9), meaning that the efforts to characterize stem cells can themselves change the characteristics of the cells. One potentially powerful approach to avoid application of extrinsic labels is to use intrinsic fluorescence signals. Some well-characterized contributors to cellular fluorescence are the intrinsically fluorescent metabolic intermediates, Nicotinamide Adenine Dinucleotide (NADH) and Flavin Adenine Dinucleotide (FAD). We have focused our current efforts on NADH, due to its key role as a carrier of electrons involved in many important metabolic pathways, including glycolysis (10), the tricarboxylic acid cycle, and the electron transport chain. NADH has two forms in cells: free and protein bound. Most bound NADH is found in the mitochondria while free NADH exists in both the cytoplasm and the mitochondria (11–13). NADH fluorescence intensity changes have been used to study cell metabolic activity in vitro and in vivo for many years (14–18). Recently, we demonstrated the utility of NADH fluorescence intensity as a noninvasive indicator of cell death in stem cell aggregates, measured using multiphoton excitation. In particular, we showed that the degree of stem cell death, identified by NADH intensity, at early stages of differentiation is predictive for the formation of functional cardiomyocytes (19). In a second study, we quantified changes in endogenous fluorescence occurring with pluripotent stem cell differentiation (20). We found that cellular-scale fluorescence intensity and lifetime of human embryonic stem cells decreased with differentiation. What emerged from these studies was a practical and accessible approach to evaluate, and ultimately enrich, living stem cell populations based on changes in metabolism, including changes that could be identified early in development, potentially predictive of subsequent differentiation state, that could be exploited for both research and clinical applications.

The utility of endogenous fluorescence to identify cells in a given state of differentiation requires appropriate technologies for visualizing those endogenous signals. Multiphoton laser scanning microscopy (MPLSM) is uniquely suited to detect endogenous fluorescence, particularly in intact three-dimensional structures, due to the broad tunability of its excitation sources, as well as improved deep sectioning, viability, and signal to noise compared to traditional optical approaches (21,22). Given these unique properties of MPLSM and clear benefits for stem cell imaging, we developed a novel multiphoton fluorescence excitation flow cytometry (MPFC) instrument to accurately probe cells deep in the interior of multicell aggregates or tissue constructs in an enhanced-throughput manner (23). This system can excite endogenous fluorophores, thereby avoiding the application of exogenous fluorescent labels. In addition, MPFC can analyze and sort aggregates based on multiple parameters. This multiparameter assessment is especially important for stem cells as (1) accurate characterization often relies on detection of multiple parameters [e.g., expression of at least two particular proteins (24) or fluorescence intensity and lifetime (20)] and (2) multiple parameters [e.g., individual cell health (25) and aggregate size (26)] contribute to the differentiation of stem cells. Here, we sought to validate the ability of our prototype MPFC system to noninvasively purify populations of stem cell aggregates (embryoid bodies, EBs) based on viability and differentiation potential via detection of NADH at early time points in differentiation.

Materials and Methods

Cell Lines and Culture Conditions

HM1 or D3 mouse ESCs were cultured as previously described (27). ESCs were harvested and resuspended in DMEM (company) + 10% FBS (company) (no LIF or BMP-4) at 1.6×10^4 cells/ml. This cell suspension was used to make 30 μl hanging drops over 1× phosphate buffered saline (PBS) in 100 mm Petri dishes (28). EBs were harvested 3 days after formation (day 3); this stage served as the time point for initiation of all studies described here.

Sorting of EBs Based on NADH Fluorescence Intensity Using the MPFC

HM1 EBs were harvested at day three of differentiation and subsequently treated with staurosporine (STS; Sigma Aldrich, St. Louis, MO). STS was applied to EB populations at a concentration of 500 nM for 3 h. After treatment, EBs were washed once with 1× PBS and resuspended in Dulbecco's Modified Eagles Medium plus 10% fetal bovine serum. The Ti:Sapphire laser was tuned to 780 nm, and a 457/50 nm emission filter was used to exclude confounding autofluorescence. Treated and untreated populations were analyzed separately on the MPFC before the sorting trials to determine each respective distribution of NADH fluorescence intensity. A real-time fluorescence intensity calculation (as previously described) (29) was used to determine total NADH expression per EB. Briefly, bright field images of EBs were used to identify the borders of EBs and total NADH fluorescence confined by this border was determined, thereby accounting for the non-contiguous distribution of intensity in each EB. Total NADH intensity was used to set a sorting threshold such that 95% or more of the treated population would be positively selected in the sorting trials. In this way, EBs with high NADH intensity were positively selected and diverted into the sorting port while those with relatively low NADH intensity flowed directly to the main port. After sorting, EBs from each port were collected and counted to determine sorting efficiency and enrichment ratio. Finally, EBs were plated onto 0.1% gelatin coated polystyrene dishes at a density of 1–4 EBs per cm^2 for long-term culture and assessment of beating areas (BA). EBs with at least one region exhibiting pulsing behavior akin to the beating of the heart were designated "EB with BA." The percentage of EBs with BA was simply the number of EBs with BA divided by the total number of EBs for a given treatment group.

For differentiation studies, unmanipulated D3 EBs were harvested on day three of differentiation and sorted according to the following criteria. Initially, a single threshold was set

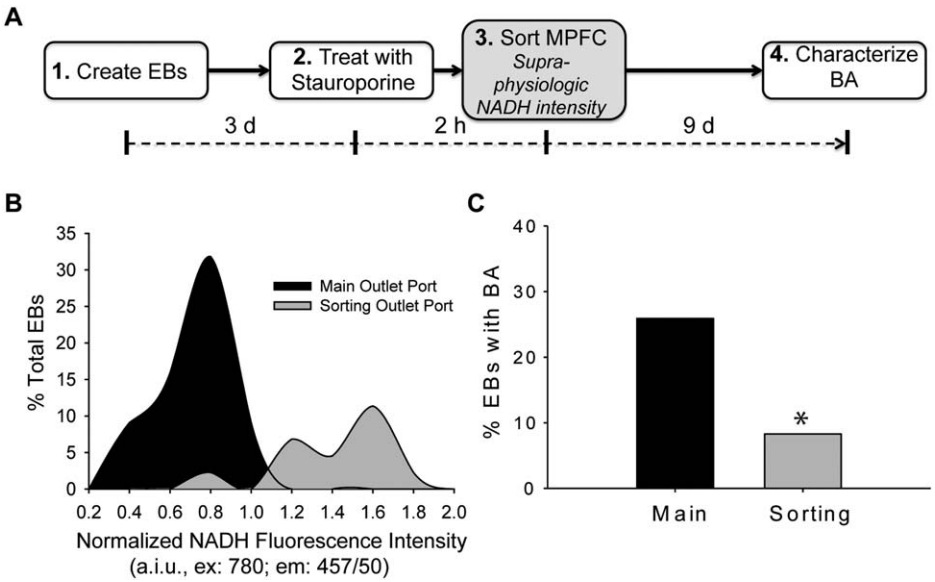

Figure 1. Enrichment of viable EBs based on NADH fluorescence intensity. **A**: EBs were harvested three days after EB formation and treated with STS (500 nM) for 2 h. EBs were then sorted based on NADH fluorescence intensity (top fifth percentile) and subsequently plated onto polystyrene dishes. Nine days after sorting (12 days post-EB formation), EBs were assessed for BA. **B**: Distribution of NADH fluorescence intensity of sorted populations on day 3 of EB formation and following STS treatment. The arbitrary intensity values were normalized to the intensity threshold for each experiment. **C**: Percentage of EBs, which produced BA in sorted populations. The percentile ranges for multiple experiments were 14–44% (Main) and 0–14% (Sorting). $*P < 0.05$. a.i.u = arbitrary intensity units.

such that the top 35% of EBs from the intensity distribution would be diverted to the sorting port (Fig. 2B). Subsequently, EBs were sorted based on both size and intensity thresholds (Fig. 2E). Size was determined as previously described[3] using the ImageJ function "Find Edges" to highlight the border of the EB using the bright field image. To ensure that small edge scan effects did not affect accurate measurement of the EB border, the "Gaussian Blur" function was used to smooth the highlighted borders in the image. Finally, a sigma radius of 2.2 was used to accurately estimate the particle size. The resulting sorted and default populations were plated onto 0.1% gelatin coated plates and allowed to proliferate and differentiate until day 12 of differentiation, when they were assessed for BA.

Statistical Analysis

For comparison of the percentage of BA between sorted and unsorted populations, Chi-squared analysis was used (Prism 5.0, GraphPad Software). Data were obtained from at least three sorting trials for each experimental design.

Results

Sorting EBs Based on NADH Fluorescence Intensity Associated with Cell Viability

We have previously shown that fluorescence intensity of NADH rises abruptly above physiologic levels following treatment with the apoptosis-inducing agent, STS, and this intensity increase corresponds to cell death in EBs (25). Here, we sought to use the NADH intensity parameters defined in that study (25) to enrich for EBs with a high percentage of viable cells and, therefore, a high percentage of cells capable of differentiating to functional mature cell types, including cardiomyocytes. To that end, EBs were formed and three days later treated with STS (500 nM) for 2 h to induce cell death (Fig. 1A). Following STS treatment, EBs were analyzed using the MPFC to determine the distribution of mean NADH intensity per population. A threshold was set at a level corresponding to the top fifth percentile of mean NADH intensity (Supporting Information Fig. S1). Cells of EBs with an NADH intensity level above this threshold were previously shown to be prone to cell death (25), therefore removal of EBs above this threshold should yield a remaining EB population enriched for viable cells. Having established a sorting intensity threshold, or gate, EBs were introduced into the MPFC for sorting. Those EBs with intensity above the threshold were diverted to the sorting port while those with intensity levels below the threshold continued to the main port (Fig. 1B). After sorting, enriched populations were placed in culture dishes and 9 days later were scored for BA (indicative of cardiomyocyte function). Indeed, those EBs exhibiting extremely high NADH intensity (above the threshold and thus diverted to the sorting port) generated significantly fewer BA (8.3%, $n = 36$ EBs) compared with the population in the main port (25.9%, $n = 81$ EBs; $P = 0.03$; Fig. 1C).

Sorting EBs Based on NADH Fluorescence Intensity as a Predictor of the Potential to Generate Cardiomyocytes

We have previously shown that EBs with high average NADH intensity at early time points after EB formation are more likely to give rise to beating cardiomyocytes at later time points than EBs with low average NADH intensity (20). To test whether NADH fluorescence intensity can serve as a predictive indicator of cardiac differentiation in EBs, we analyzed

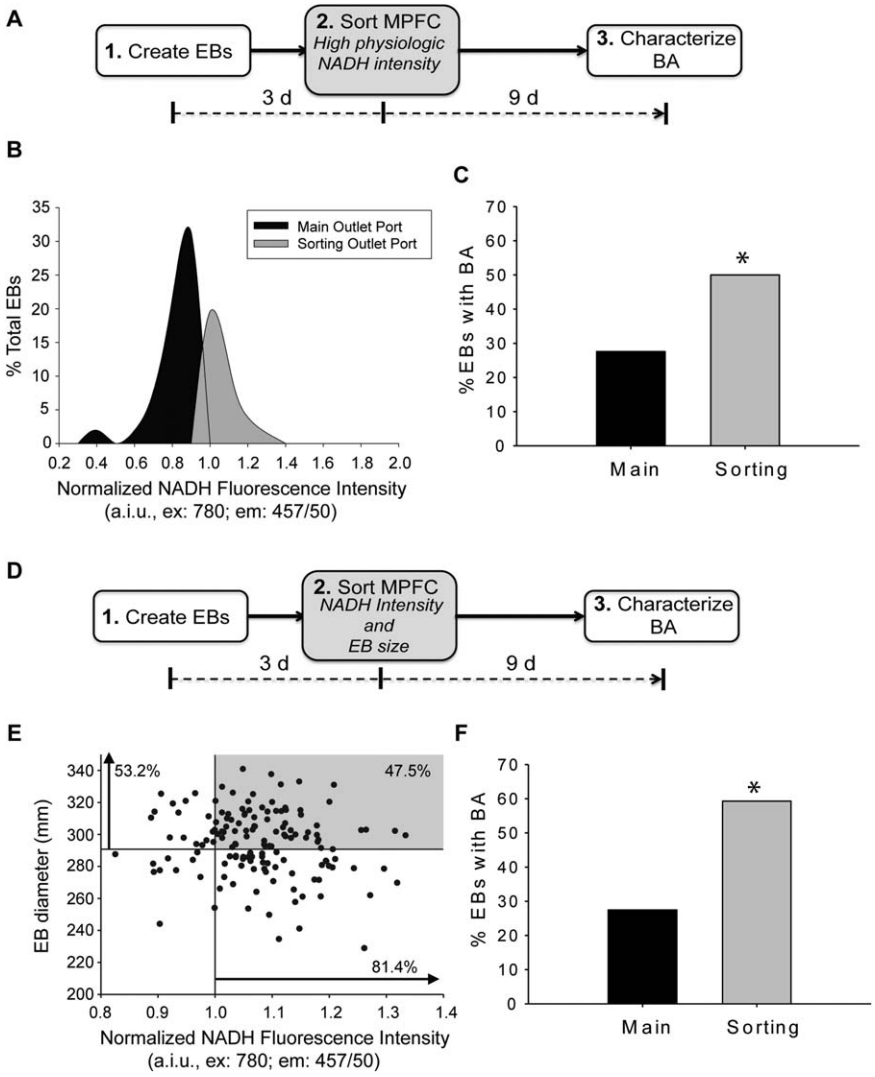

Figure 2. Enrichment of untreated EBs more likely to give rise to cardiomyocytes based on intrinsic parameters. **A**: EBs were harvested three days after EB formation, sorted based on physiological NADH fluorescence intensity levels and subsequently plated onto polystyrene dishes. Nine days after sorting (12 days post-EB formation), EBs were assessed for BA. **B**: Distribution of NADH fluorescence intensity of EBs 3 days after formation. EBs with NADH intensity in the top 35th percentile of the distribution (gray area in histogram) were selected for sorting. The arbitrary intensity values were normalized to the intensity threshold for each experiment. **C**: Percentage of EBs exhibiting one or more BA nine days after EB sorting. The percentile ranges for multiple experiments were 16–41% (Main) and 33–60% (Sorting). **D**: EBs were harvested three days after EB formation, sorted based on both physiological NADH fluorescence intensity levels and EB size, then plated onto polystyrene dishes. Nine days after sorting (12 days post-EB formation), EBs were assessed for BA. **E**: Dot plot depicting the distribution of EB size and NADH fluorescence intensity. Threshold values were set to detect EBs in the top 50% percentile for size (vertical arrow) and in the top 80% percentile for intensity of NADH (horizontal arrow) and to sort on EBs that met both of these criterion (gray upper right quartile, corresponding to ~40% of the total population). **F**: Percentage of EBs exhibiting BA nine days after EB sorting. The percentile ranges for multiple experiments were 19–41% (Main) and 50–64% (Sorting). *$P < 0.01$. a.i.u = arbitrary intensity units.

and sorted EBs 3 days after formation based on endogenous fluorescence intensity (Fig. 2A). The sorting gate was selected such that EBs in the upper 35th percentile of intensity were positively sorted (Fig. 2B). It is important to note that the intensity distribution for untreated EBs, as used in this experiment, is much lower that the intensity distribution for EBs treated with STS (Fig. 1B, Supporting Information Fig. S1). Intensity data were normalized in each trial based on the set threshold value for that trial. After sorting, enriched populations were placed in culture dishes and 9 days later were scored for BA (indicative of cardiomyocyte function). EBs diverted to the sorting port (high physiological NADH intensity) were more likely to give rise to BA (50%, $n = 62$ EBs) than unselected EBs (low NADH intensity, main port, 27.6%, $n = 105$ EBs; $P = 0.0036$; Fig. 2C). These data support our previous work showing that EBs exhibiting higher endogenous fluorescence intensity at an early stage of differentiation has a greater propensity to produce cardiomyocytes (20).

In an effort to improve the enrichment of EBs for those that ultimately give rise to cardiomyocytes, additional

intrinsic parameters to complement analysis of metabolic status (NADH intensity) were considered. In particular, EB size is known to affect cardiomyocyte differentiation potential (26,30–33). Therefore, we tested whether sorting based on both EB size and NADH fluorescence intensity can improve the selection of EBs with a higher propensity to produce cardiomyocytes (Fig. 2D). Toward this end, we simultaneously sorted EBs with average NADH intensity in the top 75th percentile of intensity and >290 μm in diameter (top 50% percentile of size). The resultant sorted population accounted for ~40% of the total EB population (Fig. 2E). EBs sorted in this manner were more likely to develop BA (59.4%, $n = 96$ EBs) than those collected from the default port (27.5%, $n = 131$ EBs; $P < 0.0001$; Fig. 2F). This represents a nearly 10% increase in the degree of enrichment, here defined as the differential between EBs with BA in the sorting port and default port, relative to the enrichment observed after sorting based on NADH intensity only.

Discussion

Here, we show the successful use of MPFC to enrich EBs based on noninvasive indicators of stem cell potential, including NADH intensity and EB size. EBs sorted in this manner can be cultured long term without the unpredictable consequences of exogenous labels, dyes, or probes. The resulting sorted cells have many advantages for postevaluation or even clinical use because of the maintenance of their natural state. In addition, sorting of EBs can be accomplished based on subtle differences in endogenous characteristics not previously possible for large particles (>50 μm). For example, EBs sorted with a size discrimination of tens of microns show altered differentiation outcomes. This outcome has been observed previously with discrimination of hundreds of microns (26,34), but it is quite surprising that even tens of microns can impact on differentiation potential. The superior ability of the MPFC to detect weak intrinsic and extrinsic signals coupled with the ability to sort on multiple parameters marks a significant advance for the enhanced-throughput analysis and purification of large particles.

The multiphoton optics inherent to the MPFC design enable detection of other types of endogenous characteristics of cells at greater imaging depth than that afforded by single photon optics. These characteristics may include detection of intensity of other endogenously fluorescent molecules (e.g., FAD, tryptophan, elastin), fluorescence lifetime and spectral analysis endogenous fluorophores, second harmonic signals indicative of molecular asymmetry prevalent in fibrillar collagens and third harmonic generation indicative of an axial phase shift prevalent at the interface between aqueous and lipid organelles. Many of these endogenous characteristics have been correlated with changes in stem cell health or differentiation state. For example, the redox ratio (NADH/FAD) of mesenchymal stem cells undergoing adipogenic differentiation was found to be significantly lower than that of stem cells maintained in a multipotent state. Further, as cells acquired a mature adipocyte phenotype, lipid droplets could be distinguished noninvasively using third harmonic generation (35,36). In similar studies, differentiating osteoblasts were assessed for production of fibrillar collagens via second harmonic generation (37) and differentiating cardiomyocytes were distinguished using second harmonic generation associated with sarcomeric myosin (38).

Stem cell aggregates such as EBs are not the only large particles that would benefit from the ability to sort based on subtle changes of noninvasive markers of cell state. Pancreatic islets are also challenging to analyze accurately in an automated manner and equally challenging to purify. Currently, aliquot of islet suspensions are manually assessed for morphology (by eye) and viability (by dye) as representative of the population prior to clinical transplant. The suspension is discarded if the aliquot does not pass quality guidelines (39). MPFC sorting based on NADH and size or granularity would avert the inherent bias associated with manual assessment as well as loss of sample since all islets analyzed could be used if sorting is sterile while the few high quality islets present in otherwise poor samples could potentially be enriched and pooled. Similar challenges exist for basic studies of engineered tissues and model organisms, including nematodes and zebrafish, where fluorescent reporters are often used. Analyses of these small organisms might benefit from a label-free approach and the ability to probe the depth of the entire organism (40–42).

Development of the MPFC system and associated ability to enrich populations based on noninvasive markers sets the stage for future advances in large particle analysis and sorting. In particular, lifetime and spectral analysis of fluorescence is not yet possible with current MPFC used approaches in a flow setting because of the time required for acquisition. Many strategies are currently under development to increase acquisition rate including investigating line scanning approaches, and faster scanning approaches such as resonant scanning. These approaches should yield a similar imaging result and significant signal to sort on, and have the advantage of greatly increasing the flow and thus sorting rate.

New commercial flow cytometry instruments (e.g., Sony SH800 benchtop cell sorter) have recently incorporated cheap, exchangeable microfluidic flow cells at the center of the instrument, to improve accessibility and ease of use for the operator (43). Such flow cells provide unique benefits not available with more permanent (e.g., quartz) flow cells found in conventional instruments, including an easily exchangeable fluidic path to maintain sterility and avoid cross contamination, daily alignment and quality control, and more accessible troubleshooting measures during instrument failure. Our large particle sorting device possesses many of these same qualities, with the added benefit of having a completely enclosed fluidic sample path, thus alleviating exposure to air or nonsterile surfaces. In this way, the MPFC is ideally suited to transition to a clinical environment, with the potential to sort microtissues and use selected populations for therapeutic applications.

Literature Cited

1. Lin S, Tran V, Talbot P. Comparison of toxicity of smoke from traditional and harm-reduction cigarettes using mouse embryonic stem cells as a novel model for preimplantation development. Hum Reprod 2009;24:386–397.

2. Flora SJ, Mehta A. Monoisoamyl dimercaptosuccinic acid abrogate arsenic-induced developmental toxicity in human embryonic stem cell-derived embryoid bodies: Comparison with in vivo studies. Biochem Pharmacol 2009;78:1340–1349.
3. Wang Y, Mulligan C, Denyer G, Delom F, Dagna-Bricarelli F, Tybulewicz VL, Fisher EM, Griffiths WJ, Nizetic D, Groet J. Quantitative proteomics characterization of a mouse embryonic stem cell model of down syndrome. Mol Cell Proteomics. 2009;8: 585–595.
4. Kadota M, Nishigaki R, Wang CC, Toda T, Shirayoshi Y, Inoue T, Gojobori T, Ikeo K, Rogers MS, Oshimura M. Proteomic signatures and aberrations of mouse embryonic stem cells containing a single human chromosome 21 in neuronal differentiation: An in vitro model of down syndrome. Neuroscience 2004;129:325–335.
5. Evseenko D, Schenke-Layland K, Dravid G, Zhu Y, Hao QL, Scholes J, Chao X, Maclellan WR, Crooks GM. Identification of the critical extracellular matrix proteins that promote human embryonic stem cell assembly. Stem Cells Dev 2009;18:919–928.
6. Gong J, Sagiv O, Cai H, Tsang SH, Del Priore LV. Effects of extracellular matrix and neighboring cells on induction of human embryonic stem cells into retinal or retinal pigment epithelial progenitors. Exp Eye Res 2008;86:957–965.
7. Ma W, Tavakoli T, Derby E, Serebryakova Y, Rao MS, Mattson MP. Cell-extracellular matrix interactions regulate neural differentiation of human embryonic stem cells. BMC Dev Biol 2008;8:90.
8. Braydich-Stolle L, Hussain S, Schlager JJ, Hofmann MC. In vitro cytotoxicity of nanoparticles in mammalian germline stem cells. Toxicol Sci 2005;88:412–419.
9. Thomas TE, Miller CL, Eaves CJ. Purification of hematopoietic stem cells for further biological study. Methods 1999;17:202–218.
10. Berg JM, Tymoczko JL, Stryer L. Biochemistry. New York: W.H. Freeman; 2002.
11. Wakita M, Nishimura G, Tamura M. Some characteristics of the fluorescence lifetime of reduced pyridine nucleotides in isolated mitochondria, isolated hepatocytes, and perfused rat liver in situ. J Biochem 1995;118:1151–1160.
12. Blinova K, Carroll S, Bose S, Smirnov AV, Harvey JJ, Knutson JR, Balaban RS. Distribution of mitochondrial nadh fluorescence lifetimes: Steady-state kinetics of matrix nadh interactions. Biochemistry 2005;44:2585–2594.
13. Belenky P, Bogan KL, Brenner C. Nad+ metabolism in health and disease. Trends Biochem Sci 2007;32:12–19.
14. Chance B, Cohen P, Jobsis F, Schoener B. Intracellular oxidation-reduction states in vivo. Science 1962;137:499–508.
15. Pappajohn DJ, Penneys R, Chance B. Nadh spectrofluorometry of rat skin. J Appl Physiol 1972;33:684–687.
16. Zhang J, Campbell RE, Ting AY, Tsien RY. Creating new fluorescent probes for cell biology. Nat Rev Mol Cell Biol 2002;3:906–918.
17. Ramanujam N, Mitchell MF, Mahadevan A, Thomsen S, Malpica A, Wright T, Atkinson N, Richards-Kortum R. Development of a multivariate statistical algorithm to analyze human cervical tissue fluorescence spectra acquired in vivo. Lasers Surg Med 1996;19:46–62.
18. Lakowicz JR, Szmacinski H, Nowaczyk K, Johnson ML. Fluorescence lifetime imaging of free and protein-bound nadh. Proc Natl Acad Sci USA 1992;89:1271–1275.
19. Buschke DG, Squirrell JM, Fong JJ, Eliceiri KW, Ogle BM. Cell death, non-invasively assessed by intrinsic fluorescence intensity of nadh, is a predictive indicator of functional differentiation of embryonic stem cells. Biol Cell 2012;104:352–364.
20. Squirrell JM, Fong JJ, Ariza CA, Mael A, Meyer K, Shevde NK, Roopra A, Lyons GE, Kamp TJ, Eliceiri KW, et al. Endogenous fluorescence signatures in living pluripotent stem cells change with loss of potency. PLoS One 2012;7:e43708.
21. Denk W, Strickler JH, Webb WW. Two-photon laser scanning fluorescence microscopy. Science 1990;248:73–76.
22. Zipfel WR, Williams RM, Christie R, Nikitin AY, Hyman BT, Webb WW. Live tissue intrinsic emission microscopy using multiphoton-excited native fluorescence and second harmonic generation. Proc Natl Acad Sci USA 2003;100:7075–7080.
23. Buschke DG, Squirrell JM, Ansari H, Smith MA, Rueden CT, Williams JC, Lyons GE, Kamp TJ, Eliceiri KW, Ogle BM. Multiphoton flow cytometry to assess intrinsic and extrinsic fluorescence in cellular aggregates: Applications to stem cells. Microsc Microanal 2011;17:540–554.
24. Bondue A, Tannler S, Chiapparo G, Chabab S, Ramialison M, Paulissen C, Beck B, Harvey R, Blanpain C. Defining the earliest step of cardiovascular progenitor specification during embryonic stem cell differentiation. J Cell Biol 2011;192:751–765.
25. Buschke DG, Squirrell JM, Fong JJ, Eliceiri KW, Ogle BM. Cell death, non-invasively assessed by intrinsic fluorescence intensity of nadh, is a predictive indicator of functional differentiation of embryonic stem cells. Biol Cell 2012;104:352–364.
26. Mohr JC, Zhang J, Azarin SM, Soerens AG, de Pablo JJ, Thomson JA, Lyons GE, Palecek SP, Kamp TJ. The microwell control of embryoid body size in order to regulate cardiac differentiation of human embryonic stem cells. Biomaterials 2010;31: 1885–1893.
27. Buschke DG, Squirrell JM, Ansari H, Smith MA, Rueden CT, Williams JC, Lyons GE, Kamp TJ, Eliceiri KW, Ogle BM. Multiphoton flow cytometry to assess intrinsic and extrinsic fluorescence in cellular aggregates: Applications to stem cells. Microsc Microanal 2011;17:540–554.
28. Maltsev VA, Rohwedel J, Hescheler J, Wobus AM. Embryonic stem cells differentiate in vitro into cardiomyocytes representing sinusnodal, atrial and ventricular cell types. Mech Dev 1993;44:41–50.
29. Buschke DG, Vivekanandan A, Squirrell JM, Rueden CT, Eliceiri KW, Ogle BM. Large particle multiphoton flow cytometry to purify intact embryoid bodies exhibiting enhanced potential for cardiomyocyte differentiation. Integr Biol (Camb) 2013; 5:993–1003.
30. Bratt-Leal AM, Carpenedo RL, McDevitt TC. Engineering the embryoid body microenvironment to direct embryonic stem cell differentiation. Biotechnol Prog 2009;25: 43–51.
31. Burridge PW, Anderson D, Priddle H, Barbadillo Munoz MD, Chamberlain S, Allegrucci C, Young LE, Denning C. Improved human embryonic stem cell embryoid body homogeneity and cardiomyocyte differentiation from a novel v-96 plate aggregation system highlights interline variability. Stem Cells 2007;25:929–938.
32. Carpenedo RL, Seaman SA, McDevitt TC. Microsphere size effects on embryoid body incorporation and embryonic stem cell differentiation. J Biomed Mater Res A 2010;94:466–475.
33. Choi YY, Chung BG, Lee DH, Khademhosseini A, Kim JH, Lee SH. Controlled-size embryoid body formation in concave microwell arrays. Biomaterials 2010;31:4296–4303.
34. Lillehoj PB, Tsutsui H, Valamehr B, Wu H, Ho CM. Continuous sorting of heterogeneous-sized embryoid bodies. Lab Chip 2010;10:1678–1682.
35. Chang T, Zimmerley MS, Quinn KP, Lamarre-Jouenne I, Kaplan DL, Beaurepaire E, Georgakoudi I. Non-invasive monitoring of cell metabolism and lipid production in 3d engineered human adipose tissues using label-free multiphoton microscopy. Biomaterials 2013;34:8607–8616.
36. Mouras R, Bagnaninchi PO, Downes AR, Elfick AP. Label-free assessment of adipose-derived stem cell differentiation using coherent anti-stokes raman scattering and multiphoton microscopy. J Biomed Opt 2012;17:116011.
37. Flausse A, Henrionnet C, Dossot M, Dumas D, Hupont S, Pinzano A, Mainard D, Galois L, Magdalou J, Lopez E, et al. Osteogenic differentiation of human bone marrow mesenchymal stem cells in hydrogel containing nacre powder. J Biomed Mater Res A 2013;101:3211–3218.
38. Awasthi S, Matthews DL, Li RA, Chiamvimonvat N, Lieu DK, Chan JW. Label-free identification and characterization of human pluripotent stem cell-derived cardiomyocytes using second harmonic generation (shg) microscopy. J Biophotonics 2012; 5:57–66.
39. Friberg AS, Lundgren T, Malm H, Felldin M, Nilsson B, Jenssen T, Kyllonen L, Tufveson G, Tibell A, Korsgren O. Transplanted functional islet mass: Donor, islet preparation, and recipient factors influence early graft function in islet-after-kidney patients. Transplantation 2012;93:632–638.
40. Gallardo VE, Behra M. Fluorescent activated cell sorting (facs) combined with gene expression microarrays for transcription enrichment profiling of zebrafish lateral line cells. Methods 2013;62:226–231.
41. Haenni S, Ji Z, Hoque M, Rust N, Sharpe H, Eberhard R, Browne C, Hengartner MO, Mellor J, Tian B, et al. Analysis of c. Elegans intestinal gene expression and polyadenylation by fluorescence-activated nuclei sorting and 3'-end-seq. Nucleic Acids Res 2012;40:6304–6318.
42. Rezai P, Salam S, Selvaganapathy PR, Gupta BP. Electrical sorting of caenorhabditis elegans. Lab Chip 2012;12:1831–1840.
43. O'Neill M. Democratizing flow cytometry. Genet Eng Biotechnol News 2013;33:12: 14–15.